# Cyano-Functionalized Triarylamines on Coinage Metal Surfaces

Müller, Kathrin; Moreno-Lopez, Juan Carlos; Gottardi, Stefano; Meinhardt, Ute; Yildirim, Handan; Kara, Abdelkader; Kivala, Milan; Stöhr, Meike

*Published in:*
Chemistry : a European Journal

*DOI:*
10.1002/chem.201503205



*Publication date:*
2016

# Cyano-Functionalized Triarylamines on Coinage Metal Surfaces: Interplay of Intermolecular and Molecule-Substrate Interactions

Kathrin Müller,[a]†* Juan-Carlos Moreno-López,[a] Stefano Gottardi,[a] Ute Meinhardt,[b] Handan Yildirim,[c] Abdelkader Kara,[c] Milan Kivala,[b]* and Meike Stöhr[a]*

## Abstract:

The self-assembly of cyano-functionalized triarylamine derivatives on Cu(111), Ag(111), and Au(111) was studied by means of scanning tunnelling microscopy, low-energy electron diffraction, X-ray photoelectron spectroscopy, and density functional theory calculations. Different bonding motifs such as antiparallel dipolar coupling, hydrogen bonding, and metal-coordination were observed. While on Ag(111) only one hexagonally close-packed pattern stabilized by hydrogen bonding is observed, on Au(111) two different partially porous phases are present at submonolayer coverage stabilized by dipolar coupling, hydrogen bonding and metal coordination. In contrast to the self-assembly on Ag(111) and Au(111), for which large islands are formed, on Cu(111), only small patches of hexagonally close-packed networks stabilized by metal coordination, and areas of disordered molecules are found. The significant variety in the molecular self-assembly of the cyano-functionalized triarylamine derivatives on these coinage metal surfaces is explained by differences in the molecular mobility as well as the subtle interplay between intermolecular and molecule-substrate interactions.

[a] Dr. K. Müller, Dr. J.C. Moreno-Lopez, S. Gottardi, Prof. Dr. M. Stöhr
Zernike Institute for Advanced Materials
Nijenborg 4
9747AG Groningen, the Netherlands
E-mail: k.mueller@fkf.mpg.de, m.a.stohr@rug.nl
Fax: +31 50 363 7208
† Current Address:
Max Planck Institute for Solid State Research
Heisenbergstrasse 1
70569 Stuttgart
Germany
[b] U. Meinhardt, Dr. M. Kivala
Chair of Organic Chemistry 1,
Department of Chemistry and Pharmacy,
University of Erlangen-Nürnberg,
Henkestrasse 42, 91054 Erlangen, Germany
E-mail: milan.kivala@fau.de
Fax: +49 9131 8526865
[c] Dr. H. Yildirim, Prof. A. Kara,
Department of Physics,
University of Central Florida,
Orlando, Florida 32816, USA

Supporting information for this article is given via a link at the end of the document.

## Introduction

The self-assembly of organic molecules on metallic surfaces has attracted increasing interest over the last two decades in fundamental research as well as for potential applications in organic devices like organic photovoltaics, organic field-effect transistors or as sensors.[1] Molecular self-assembly is based on the concepts of supramolecular chemistry, where non-covalent intermolecular interactions[2] like hydrogen bonding (H-bonding),[3] dipolar coupling,[4,5] π-π stacking[6] or metal coordination[7] are employed to create supramolecular architectures.[8] Highly organized and defect-free structures can be realized because of self-recognition and error correction, that happen via bond breaking and bond formation until an equilibrium structure is formed.

Besides the intermolecular interactions, which can be controlled via specific functional groups, molecular self-assembly on surfaces also depends on the molecule-substrate interactions, which are influenced by the reactivity of the substrate, the crystal structure, the corrugation of the adsorption potential, and potential surface reconstructions. Often subtle differences between intermolecular and molecule-substrate interactions can lead to significant differences in the self-assembly and electronic properties of the same molecule on different surfaces.[9-11] For example, the adsorption of 3,4,9,10-perylenetetracarboxylic acid dianhydride (PTCDA) on Cu(111) and Ag(111) leads to a charge transfer from the substrate to the molecule resulting in a filling of the lowest unoccupied molecular orbital (LUMO), while on Au(111) the LUMO remains empty.[11] It was also shown that deposition of metal-free tetraphenyl porphyrins on Cu(111) leads to mostly isolated molecules due to the strong interaction of the iminic nitrogen atoms with the copper surface, while deposition of the same molecules on Ag(111) results in well-ordered islands because of a weaker molecule-substrate interaction.[12] For fullerenes ($C_{60}$) on noble metal surfaces the self-assembly and the molecular orientation are determined by a subtle interplay between the intermolecular and molecule-substrate interactions. While the spacing between the $C_{60}$ molecules is always around 1.0 nm – similar to the (111) bulk lattice spacing of $C_{60}$ – subtle differences in the rotational mobility, orientation and layer growth were observed on gold, silver and copper.[13] These differences can be explained by either surface

reconstructions like on Au(111) and Au(110) or by the differences in the reactivity of the surfaces.[13]

The study of molecular self-assembly of organic molecules functionalized with cyano groups is particularly interesting because the asymmetric charge distribution of the cyano group with the negatively polarized N-atom leads to the formation of a local internal dipole. The cyano group cannot only participate in H-bonding and dipolar coupling, but it can also efficiently coordinate to a variety of metals.[14-17] Different molecular patterns like 0D clusters, 1D chains and 2D islands can be created by changing the number of cyano groups and/or their relative position, as it was demonstrated for cyano-functionalized porphyrin and polyphenylene derivatives.[4,14,18]

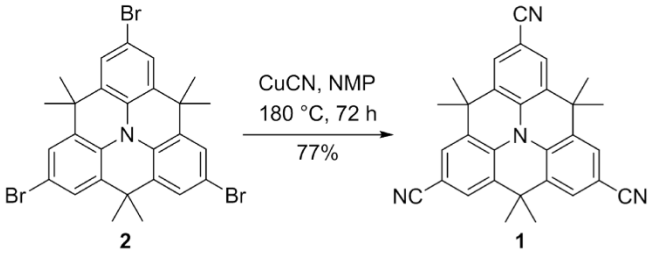


**Scheme 1.** Synthesis of the cyano-functionalized triarylamine derivative **1**. NMP = *N*-methyl-2-pyrrolidone. See Experimental Details for further details.

In this study, we report on the self-assembly of a cyano-functionalized planarized triarylamine derivative, (4,4,8,8,12,12-hexamethyl-4*H*,8*H*,12*H*–benzo[1,9]quinolizino[3,4,5,6,7-*defg*]acridine-2,6,10-tricarbonitrile) denoted as **1** on coinage metal (111) surfaces (Scheme 1). Such planarized triarylamines, so-called heterotriangulenes, are at present of growing interest owing to their potential as stable electron-rich building blocks for optoelectronic organic materials.[19,20] In our recent study on the self-assembly of **1** on Au(111), we could show that the molecules can undergo H-bonding, dipolar coupling, and metal-ligand interaction.[21] By comparing these results to the self-assembly on Ag(111) and Cu(111), we aim to provide insight into the subtle interplay between molecule-substrate and intermolecular interactions leading to significant differences in the self-assembled patterns. We show that the molecule-substrate interaction, the surface reconstruction (e.g. of Au(111)), the molecular mobility and the intermolecular interactions determine the sizes and the structures of the molecular patterns.

## Results

### *Scanning tunnelling microscopy measurements*

In order to identify the orientation of the individual molecules with the scanning tunnelling microscope, we have to note that triarylamine derivatives containing out of plane bridging methyl groups on metal surfaces usually exhibit three protrusions in scanning tunnelling microscopy (STM) images, giving rise to a triangular appearance of the molecules (see Figure S2 in the Supporting Information). This triangular shape arises from the out of plane bridging methyl groups, while the cyano groups of the molecule are not imaged.[21,22] This allows to determine the molecular orientation within the adsorbate structures. Submonolayer coverage of **1** on Ag(111) leads to the formation of islands – up to several hundreds nm in size – which often grow over the step edges (see Figures S3 and S4a in the Supporting Information). Figure 1a presents a molecularly resolved STM image taken on such an island, which shows that the molecules assemble in a well-ordered hexagonally close-packed pattern. Generally, the molecules are oriented in the same direction with one of their three vertexes (i.e. one dimethylmethylene ($C(CH_3)_2$ group) pointing to the top. However, some molecules are rotated by 180°, i.e. with one vertex pointing down – exemplarily two are marked by black circles in Figure 1a.

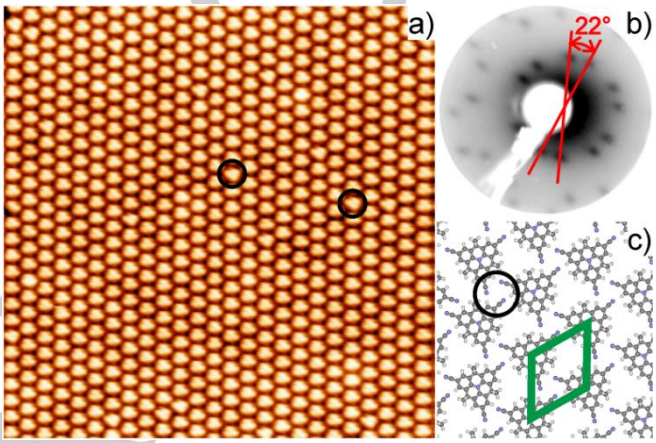


**Figure 1.** Close-packed structure of **1** on Ag(111). a) STM image (25x25 nm$^2$, $U$ = –2.0 V, $I$ = 30 pA). The black circles indicate exemplarily two molecules, which are rotated by 180° with respect to the other molecules. b) LEED pattern taken at an incident electron energy of 35 eV. The angle between two chirally different domains is marked in red. c) Tentative model of the molecular arrangement with the unit cell marked in green. The black circle highlights the trimeric H-bonding motif.

Figure 1c shows the tentative structure model of the molecular arrangement derived from the STM as well as from the low-energy electron diffraction (LEED) measurements (Figure 1b). The unit cell – marked in green in Figure 1c – has a size of 1.32x1.32 nm$^2$ and an internal angle of 120°. The cyano group of one molecule points to the phenyl hydrogen of a neighbouring molecule leading to a hydrogen-bonding motif (C≡N···H), which is well known for other molecules containing cyano functionalized phenyl rings.[23] Because three neighbouring molecules are involved in such a C≡N···H interaction (see black circle in Figure 1c), we name this a trimeric bonding motif. This C≡N···H interaction induces organizational chirality[24]: the N-atom can either point to the phenyl hydrogen atom on the left side of the methyl groups of the neighbouring molecule as shown in Figure 1c or to the right side (not shown here). Consequently, two chiral domains have to exist on the surface. Thus, the two mirror domains which are revealed in the LEED pattern (Figure 1b) are due to the two different chiral domains, that are rotated by 22° with respect to each other (11° with respect to the <1$\bar{1}$0> direction of the Ag(111) substrate). Indeed, these chiral domains can also be identified in the STM images (Figure S4 in the Supporting Information). However, no domain boundaries, where the two different chiral domains meet, were observed. Thus, we assume that the molecules can easily rotate

and translate to adjust to one of the chiral arrangements when two islands with different orientation coalesce, leading to an Ostwald ripening as previously reported for organic molecules adsorbed on solid surfaces.[25]

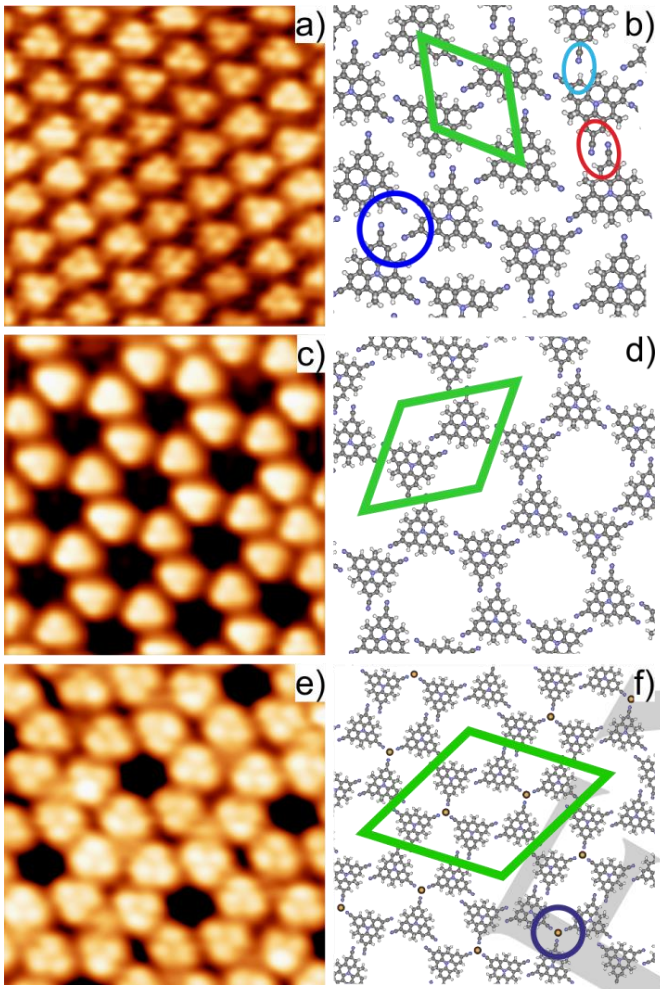


**Figure 2**. Comparison of the different phases for **1** on Au(111). a) STM image of close-packed phase *α* observed for monolayer coverage (7x7 nm$^2$, *U* = 2.8 V, *I* = 170 pA). c) STM image of porous phase *α* (7x7 nm$^2$, *U* = 2.0 V, *I* = 70 pA). e) STM image of phase *β* (7x7 nm$^2$, *U* = 3.0 V, *I* = 140 pA). b), d), f) Tentative structure models of close-packed phase *α*, porous phase *α* and phase *β*, respectively. The unit cells are marked in green, while the coloured ovals and circles indicate different bonding motifs (see text). Copyright Wiley-VCH Verlag GmbH & Co. KgaA. Reproduced with permission from Ref. 21.

Deposition of one monolayer (ML) of **1** on Au(111) results in a hexagonally close-packed pattern, called phase *α* in the following. The herringbone reconstruction of the Au(111) surface remains intact underneath the molecules.[21] The unit cell – marked in green in Figure 2b – has a size of 1.32x1.32 nm$^2$ with an internal angle of 120°. The high-resolution image in Figure 2a shows that the molecules exhibit two different orientations, which are rotated by 180° with respect to each other. Noteworthy, a correlation with the periodicity of the herringbone reconstruction has been identified for the two different molecular orientations.[21] From the tentative structure model in Figure 2b, it becomes apparent that the different molecular orientations lead to two specific interaction motifs: (i) An antiparallel dipolar coupling motif where the cyano groups of neighbouring molecules are oriented parallel to each other (red oval in Figure 2b), and (ii) a H-bonding motif (light blue oval in Figure 2b). The dark blue circle indicates the trimeric motif formed by three molecules undergoing H-bonding. Gas phase density functional theory (DFT) calculations using the optB86b functional showed that the different bonding motifs only vary slightly in binding energy with the dipolar coupling motif being the most stable one.[21] Similar to what was observed for **1** on Ag(111), two chiral mirror domains rotated by 11° with respect to the <1 $\bar{1}$ 0> direction of the Au(111) surface exist; their presence is also due to the fact that the cyano group can point either left or right to the phenyl hydrogen atom.[26]

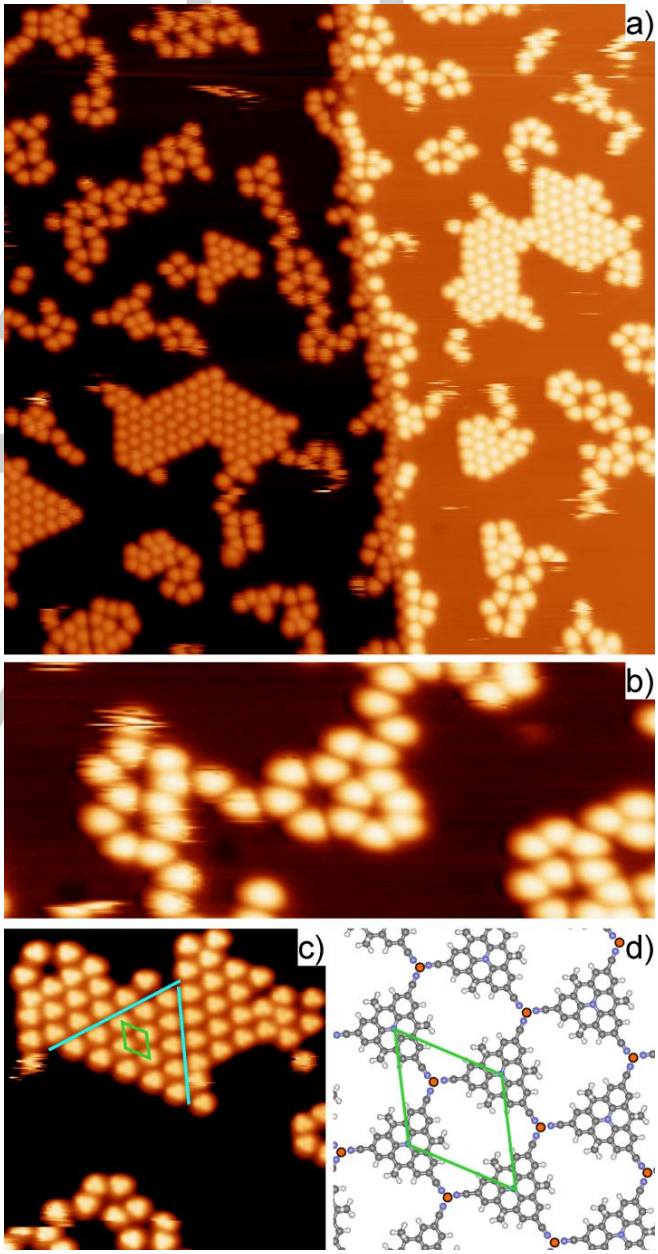


**Figure 3.** Submonolayer coverage of **1** on Cu(111). a) Overview STM image (60x60 nm$^2$, *U* = 1.0 V, *I* = 18 pA). b) Close-up STM image of a disordered area (25x10 nm$^2$, *U* = -1.0 V, *I* = 18 pA). c) Close-up STM image of an ordered island with the unit cell marked in green (20x20 nm$^2$, *U* = 1.5 V, *I* = 13 pA). The blue lines indicate domain boundaries. d) Tentative model of the molecular arrangement of the close-packed structure with the unit cell marked in green, orange spheres indicate Cu atoms.

Deposition of less than 1 ML of **1** on Au(111) leads to the coexistence of two different phases – both of them exhibit organizational chirality. Phase *α* now exhibits many pores, which assemble into a porous network (Figure 2c). Within these porous areas, neighbouring molecules are rotated by 180°, and they exclusively interact via the dipolar coupling motif, which is visible in the tentative structure model shown in Figure 2d. In addition, a second partially porous phase – called phase *β* – with a unit cell size of 3.77x3.77 nm$^2$ and an internal angle of 120° was observed (Figure 2e). While for the porous phase *α*, three neighbouring pores share one molecule, the pores in phase *β* do not share any molecules. A detailed analysis of phase *β* shows that the six molecules forming one pore interact via dipolar coupling, while bonding between the pores happens via metal-ligand interaction (Figure 2f; the metal-ligand bond is marked by the dark blue circle). For more details on the assembly of **1** on Au(111) we refer to Ref. 21.

Figure 3a shows an overview STM image acquired after deposition of submonolayer coverage of **1** on Cu(111). Small islands with a well ordered molecular arrangement are visible with a maximum island diameter on the order of 50 nm (Supporting Information Figure S5). Besides, a disordered arrangement is present, where the molecules form short rows and pores. The molecules adsorbed on both sides of the step edges on Cu(111) show a high degree of disorder, which is in contrast to what has been observed on Ag(111) (see Figure S3b and S4a in the Supporting Information) and Au(111)[21] where well-ordered patterns at the step edges are observed often leading to their restructuring.

We start with discussing the disordered areas on Cu(111), which can be seen in more detail in Figure 3b and in Figure S6 in the Supporting Information. It is worth noting that the molecules in the disordered areas tend to form a porous structure. However, most of the pores deviate from a hexagonal shape. In Figure 3b, it is evident that the flat edges of the triangularly appearing molecules are roughly parallel to each other, while there is a lateral offset between neighbouring molecules (see also Figure S6 in the Supporting Information). This specific molecular arrangement indicates that the molecules interact via dipolar coupling. We assume that the main reason for the missing long-range order is the lattice mismatch between the Cu(111) unit cell and the unit cell of a regular hexagonal porous network formed via dipolar coupling. A strong molecule-substrate interaction prevents a more regular ordering of the molecules, because the molecules tend to maintain their preferred adsorption position and orientation with respect to the substrate.

A close inspection of the ordered islands (Figure 3c) shows that neighbouring molecules have the same orientation. However, some domain boundaries where the molecules are rotated by 180° with respect to their neighbouring molecules are also present (see light blue lines, indicating two domain boundaries in Figure 3c). These domain boundaries are mostly stabilized by antiparallel dipolar coupling. Noteworthy, the close-packed islands on Cu(111) are mostly oriented parallel to the close-packed <1$\bar{1}$0> direction of the Cu(111) surface. This observation is also confirmed by the LEED pattern where no rotational domains have been observed for **1** on Cu(111) (Figure S7 in the Supporting Information).

Comparing the close-packed patterns on Cu(111) with those observed on Ag(111) and Au(111), some subtle differences can be recognized. First, the unit cell on Cu(111) (1.4x1.4 nm$^2$) is slightly larger than the unit cell on Ag(111) or Au(111) (1.32x1.32 nm$^2$). The unit cell dimensions are 5.5 times the nearest neighbour distance of the Cu(111) substrate (0.255 nm). Thus, we assume that the close-packed network on Cu(111) forms a coincidence lattice,[27] which can be described by an (11 x 11) superstructure containing four molecules. Second, while the edges of the molecular triangles are slightly rotated away from the unit cell directions on Ag(111) and Au(111), they are parallel to the unit cell directions on Cu(111) (see the tentative structure models in Figure 1c, 2b, 3d and Figure S8 in the Supporting Information). A careful inspection of Figure 3c reveals that the cyano groups in the close-packed network on Cu(111) point towards each other (Figure 3d). As this orientation is energetically unfavourable due to the repulsion between the partially negatively charged N-atoms, we assume that the molecular network is stabilized by metal-ligand bonding with native copper atoms. Such metal-coordination bonds between cyano groups and native copper atoms were reported for example for cyano-functionalized porphyrin or helicene molecules on Cu(111).[14,15] Although, the coordinating metal atom is generally not visible in STM, enhanced contrast is visible at the position of the coordinating metal atom under specific tunnelling conditions, which is generally assumed to be a signature for metal coordination (Figure S8a in the Supporting Information).[21,28,29]

### *X-ray photoelectron spectroscopy (XPS) measurements*

To further confirm the assumption of a metal-ligand bonded network on Cu(111) in contrast to a hydrogen bonded / dipolar coupled network for the close-packed phase *α* on Au(111), we performed XPS measurements of the N1s region for multilayer and submonolayer coverage of **1** on both Au(111) and Cu(111) (see Figure 4 and Table 1). For the multilayer spectra on Au(111) and Cu(111), respectively, two peaks can be distinguished (Figure 4, top spectra).[30] The peak at 399.4 eV can be assigned to the nitrogen of the cyano groups, and its binding energy is comparable to what has been reported for other cyano-substituted molecules.[31,32] The peak slightly above 401 eV can be assigned to the central N-atom of the triphenylamine unit (Scheme 1). The area ratio of the two N1s peaks (central N/cyano N) is 1:2.8 on Au(111) and 1:3 on Cu(111), which is close to the theoretical value of 1:3. After deposition of 0.85 ML on Au(111), the same two peaks are observed. However, the peaks are shifted slightly towards lower binding energies, which we assign to final state effects and possible changes in the work function. Note, that for this sample mostly phase *α* was observed in STM, where the molecules undergo dipolar coupling and H-bonding, but no metal coordination. In contrast, for 0.85 ML on Cu(111) a clear shoulder at lower binding energies is observed. This spectrum can only be fitted with three components. The peak around 400.5 eV can again be assigned to the central N-atom, and only shifts slightly with respect to the multilayer spectrum similar to what was observed for **1** on Au(111). The peak around 399 eV

has a similar binding energy as the one at lower binding energy on Au(111) for 0.85 ML of **1** and thus, can be related to the N-atom of the cyano group undergoing H-bonding or dipolar coupling. The peak at 397.5 eV can be related to a C≡N···Cu metal-ligand interaction. Note, that the ratio of the area between the peak at highest binding energy (triphenylamine unit) to the two peaks assigned to the cyano N-atom is 1:3.1, which is very close to the stoichiometric value. A shift to lower binding energy for metal coordinated cyano N-atoms was reported for tetracyanoquinodimethane (TCNQ) on Cu(100) and its coordination to Mn. The N1s binding energy for the metal coordinated TCNQ is higher (398.7 eV) than the one reported here, however the trend is the same.[31,33] Thus, the XPS data add further evidence for the metal-ligand interaction of **1** to native Cu atoms on Cu(111). Note, that for the sample measured, both phases (the close-packed as well as the disordered phase) were observed in STM. Thus, the peak at 399.2 eV can be assigned to the molecules in the disordered areas, which are mostly stabilized by dipolar-coupling.

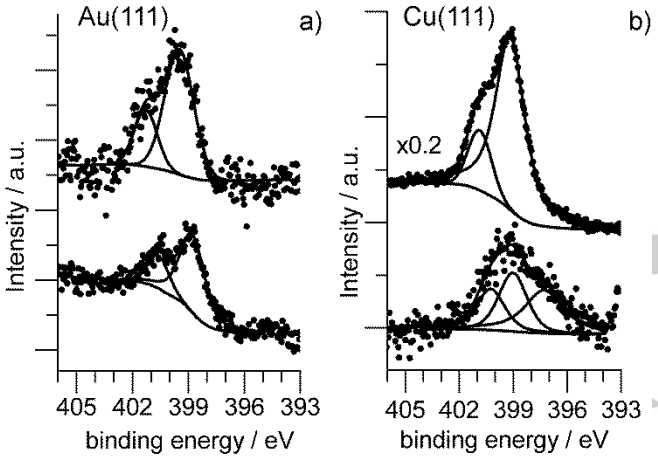


**Figure 4.** N1s XPS spectra taken on Au(111) (a) and on Cu(111) (b) for multilayer coverage of **1** (top, 4 ML on Au(111) and 6 ML on Cu(111)) and 0.85 ML of **1** (bottom). The dotted lines indicate the measured data, while the thin black lines represent the fits. The spectrum for multilayer coverage on Cu(111) was multiplied by a factor of 0.2 for better visibility.

**Table 1.** N1s binding energies and the ratio of the peak areas for multilayer and submonolayer coverage of **1** on Au(111) and Cu(111), respectively.

| | $E_B$ [eV] $NC_3$ | $E_B$ [eV] C≡N···H | $E_B$ [eV] C≡N···Cu | ratio |
|---|---|---|---|---|
| 4 ML / Au(111) | 401.3 | 399.5 | | 1:2.8 |
| 0.85 ML / Au(111) | 400.6 | 398.8 | | 1:3.4 |
| 6 ML / Cu(111) | 401.1 | 399.4 | | 1:3.0 |
| 0.85 ML / Cu(111) | 400.5 | 399.2 | 397.5 | 1:1.7:1.4 |

## *Computational results*

To gain further insight into the molecule-substrate interactions, which seem to play a prominent role in the self-assembly of **1** on the coinage metal surfaces, we performed DFT calculations including van der Waals interactions via the optB88-vdW functional. The choice of the optB88-vdW functional is based on recent detailed studies of molecular adsorption on several metal surfaces.[34] The adsorption energies were calculated for three different adsorption configurations for each of the three surfaces investigated. The configurations were chosen in such a way that the molecules' inner rings coincide with a substrate atom, a bridge or a hollow site. The calculated adsorption energies vary between 2.62 eV and 2.73 eV for Ag, 2.82 eV and 3.06 eV for Cu, and 2.92 eV and 3.50 eV for Au. In Table 2 and Figure 5, the most stable adsorption configuration for each surface is reported.

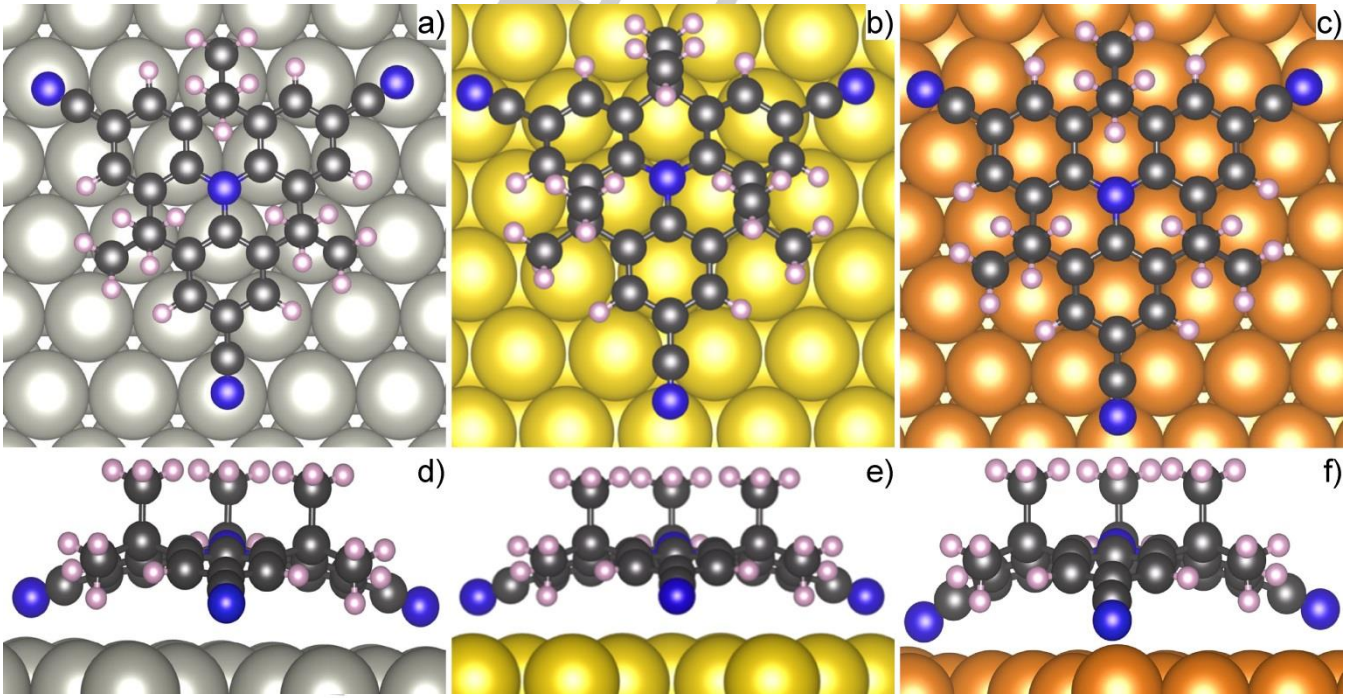


**Figure 5.** Most stable adsorption configurations of **1** on Ag(111) (a, d), Au(111) (b, e) and Cu(111) (c, f). The side views (d, e, f) show the strong arching of **1**. Colour code: light grey: Ag, yellow: Au, orange: Cu, blue: N, dark grey: C, light pink: H.

The results of the DFT calculations for a single molecule adsorbed on either Au(111), Ag(111), and Cu(111) show a strong arching of the molecule, *i.e.* a bending of the cyano groups towards the surface, while the methyl groups are rotated away from the surface (see Figure 5 and Table 2). The angle between the two methyl groups amounts to 108°, similar to the angle obtained from x-ray structure analysis for similar triarylamines.[20] Additionally, on Cu(111) an out-of-surface displacement of the Cu-atom underneath the N-atom of the cyano group of approximately 0.2 Å is observed, while neither the Ag nor the Au surface undergo any noticeable restructuring. The stronger N-Cu interaction also manifests itself in a stronger overlap of the van der Waals radii of the N and Cu atoms[35] compared to **1** on either Ag(111) or Au(111) (Table 2). Astonishingly, the stronger interaction of the molecule with the Cu surface leads only to a slightly larger binding energy compared to Ag(111) while it is even smaller than for Au(111).[36] The reason for the comparably lower binding energy on Cu(111) could be that the strong arching and buckling is energy consuming and consequently the total energy of the most stable configuration is lower than that for for Au(111). Note that for calculating the total binding energy, the energy of the flat molecule in gas phase and of the undistorted surface are used. Furthermore, the unreconstructed gold surface was used in the calculations, which might lead to slightly higher adsorption energy as the stress that is induced in the gold surface due to the missing reconstruction might be partly reduced by the adsorption of the molecule.

**Table 2**. Binding energy, arching (Figure S1 in the Supporting Information), shortest distance between the metal atom (M) and the N-atom (N) of the cyano group ($d_{M\text{-}N}$), overlap of the van der Waals radii $d_{vdW} = d_{M\text{-}N} - d_{vdW,M} - d_{vdW,N}$ [35] and displacement of the metal atoms (buckling) are presented for Ag(111), Au(111) and Cu(111).

| Surface | $E_{bind}$(eV) | Arching | $d_{M\text{-}N}$ (Å) | $d_{vdW}$(Å) | Buckling (Å) |
|---|---|---|---|---|---|
| Ag(111) | 2.73 | 156° | 2.54 | -0.73 | 0.02 |
| Au(111) | 3.50 | 157° | 2.58 | -0.63 | 0.04 |
| Cu(111) | 3.06 | 148° | 2.08 | -0.87 | 0.20 |

## Discussion

In the following, we will address the remarkable differences of the self-assembled patterns observed for **1** on the three (111)-oriented coinage metal surfaces. It is well known that the surface-confined molecular self-assembly depends mostly on (i) the mobility of the molecules on the surface, (ii) the competition between intermolecular and molecule-substrate interactions and (iii) the thermal energy brought into the system, among others.[37] As the molecules were deposited with the samples kept at room temperature and all of the STM measurements shown in the main part of the paper were performed at 77 K, the thermal energy gained by the molecules is similar for the different cases and thus, will not be considered further.

It is obvious from the STM images, that the molecular islands on Cu(111) are considerably smaller than on Au(111) and Ag(111), respectively. This can be explained by taking into account the first factor mentioned above, namely the mobility of the molecules. We assume that the molecules are much less mobile on Cu(111) compared to Au(111) and Ag(111), respectively, and thus only small islands – less than 50 nm in size – are present for submonolayer coverage on Cu(111). Furthermore, on Cu(111) often domain boundaries in the ordered patches were found while no domain boundaries were observed for the different chiral domains on Au(111) and Ag(111), respectively. This is astonishing because different islands probably coalesce during their growth. Thus, the absence of domain boundaries on Au(111) as well as on Ag(111) can be related to a higher molecular mobility: Even within the islands, the molecules can easily rotate and translate in order to adjust to one of the chiralities, while on Cu(111) the rotation of the molecules seems to be hindered. Similar differences in the mobility and thus in the size and shape of molecular patterns on Cu, Ag, and Au have been reported earlier.[12,37] For example, the adsorption of submonolayer coverages of metal-free tetraphenyl porphyrin molecules at room temperature leads to close-packed patterns on Ag(111), while isolated molecules are found on Cu(111) due to the strong interaction of the iminic N-atoms with the copper surface.[12] Thus, we assume that the reduced mobility and the preference of specific adsorption positions for **1** on Cu(111) due to the strong molecule-substrate interaction compared to Ag(111) and Au(111) is the most important factor determining the island sizes.

The second factor – the interplay between intermolecular and molecule-substrate interactions – is more difficult to access. Especially, as different intermolecular interactions are present on the different surfaces. Recently, we reported that **1** can undergo (I) H-bonding, (II) dipolar coupling, and (III) metal coordination.[21] First we want to compare the bonding motifs (I) and (II) for Au(111) and Ag(111). Gas phase calculations showed that the dipolar coupling motif is slightly more stable than the trimeric motif and a single hydrogen bond is the least stable.[21] Besides the similarities of the hexagonally close-packed networks of **1** on Ag(111) and Au(111), like the same unit cell parameters and orientation, some subtle differences in the intermolecular interactions are observed, which we believe to originate from the different molecule-substrate interactions. Note, that the lattice constants of Au(111) and Ag(111) are similar (4.07 Å for the unreconstructed Au and 4.09 Å for Ag). While on Ag(111) the molecules interact exclusively via H-bonding, on Au(111) both, H-bonding and dipolar coupling interactions, are found in phase *α*. Generally, molecules tend to pack in the densest arrangement possible in order to reduce the surface free energy. To achieve this goal, different options are possible for the molecules studied. Either all molecules are oriented in the same direction and the hexagonal close-packed network is stabilized exclusively by H-bonding, as observed for Ag(111) (Figure 1a and c), or the molecules adopt two different orientations (rotated by 180° with respect to each other) and consequently interact via dipolar coupling and H-bonding. The latter option is the case for the close-packed arrangement on Au(111) (Figure 2a and b). We can only speculate about the reasons why the network on Ag(111) and Au(111) are formed by different intermolecular interactions. We found that the herringbone reconstruction of the Au(111) surface, which is preserved underneath the molecules, plays a subtle role for the molecular orientation with respect to the surrounding molecules.

Specifically, we observed a correlation of the orientation of the molecules with a periodicity similar to the one of the herringbone reconstruction.[21] Thus, we assume that the herringbone reconstruction and more specifically the alternating *hcp*- and *fcc*-sites influence the orientation of neighbouring molecules. This could explain the differences in the bonding motifs on Au(111) and Ag(111) for the – on the first glance identical – hexagonally close-packed patterns. A second significant difference for the structures observed on Au(111) and Ag(111) are the porous superstructures, found for less than one monolayer coverage on Au(111), while the pattern on Ag(111) did not exhibit any pores, even for low coverages. We assume that the presence of a hexagonally porous structure on Au(111) is also favoured by the underlying herringbone reconstruction. Note, that the pores are exclusively formed by dipolar coupling interactions, which are also present in the close-packed structure on Au(111), while on Ag(111) the molecules interact exclusively via H-bonding.

Besides H-bonding and dipolar coupling, metal-coordination interactions were found on Cu(111) as well as Au(111). While there are examples for metal-coordination of cyano containing molecules with native ad-atoms on Cu(111)[14,33] and Au(111)[38] surfaces, to the best of our knowledge metal-coordinated networks on Ag(111) surfaces with native ad-atoms have not been reported, yet. However, recently it was shown that copper-phthalocyanine molecules can coordinate to native Ag atoms on a Ag(100) surface.[39] Furthermore, the coordination of cyano-functionalized molecules to silver atoms in solution in 3D metal-organic frameworks (MOFs) has been reported earlier.[40] Sirtl et al. showed that the bond dissociation energy of two benzonitrile molecules on a silver surface binding to a silver atom is considerably lower than the one calculated for a similar bond involving a copper atom on a copper surface.[17] Thus, we assume that the lack of metal coordination on Ag(111) is due to a lower bond energy of the CN···Ag bond on the silver surface in comparison to a CN···Cu bond on a copper surface. This is in line with our DFT calculations which show a much stronger bending of the molecule and a larger overlap of the van der Waals radii for the Cu surface compared to the Ag surface (Table 2).

The reduced island size for **1** on Cu(111), the buckling of the first metal layer and the distortion of the molecules indicate that the molecule-substrate interaction for Cu(111) is the strongest, while it is the weakest for Ag(111). This is contradicting the binding energies calculated by DFT (see Table 2) where the following sequence is observed: Ag < Cu < Au. This example shows that one has to be careful comparing solely binding energies obtained from DFT calculations. First, a strong interaction, which leads to a distortion of the molecule as well as of the surface, can result in a too small total binding energy – as it is the case for **1** on Cu(111) – because the energy which is consumed by the surface restructuring and buckling of the molecules is not taken into account in the DFT calculations. Second, the calculations for a Au(111) surface always have to be taken with care as the herringbone reconstruction is not considered, leading to additional stress in the gold surface, which might be reduced by the adsorption of molecules leading to a too high binding energy. Last but not least our calculations were done for isolated molecules, i.e. not considering intermolecular interactions. It is possible that the arching of the molecules is reduced if they undergo dipolar coupling or H-bonding. However, the arching of a single molecule, the displacement of the underlying Cu metal atom and the overlap of the van der Waals radii provide additional insight into the molecule-substrate interactions and help in the interpretation of our experimental observations.

## Conclusions

We studied the self-assembly of a cyano functionalized, planarized triarylamine derivative **1** for submonolayer to monolayer coverage on coinage metal surfaces. Three different intermolecular interactions – dipolar coupling, H-bonding, and metal coordination – were found. On Ag(111) – independent of the coverage – a hexagonally close-packed phase, where the molecules interact exclusively via H-bonding, exists. In contrast, on Au(111) two well-ordered phases stabilized by all three possible bonding motifs were observed for submonolayer coverage. On Cu(111), only small patches of ordered molecules stabilized by metal-coordination bonding exist together with areas of disordered molecules, which interact mostly via dipolar coupling.

We suggest that the molecular mobility as well as the molecule-substrate interaction are mainly responsible for the structure formation, while the intermolecular interaction (with the three different bonding motifs available) helps to adapt for the specific molecule-substrate interactions. The strong interactions of the cyano groups with the copper surface lead to a displacement of the copper atom underneath the N-atom and a strong arching of the molecule. We propose that the differences for the intermolecular interactions observed on Au(111) compared to Ag(111) for the close-packed structures are related to the herringbone reconstruction which leads to subtle differences in the molecule-substrate interactions on Au(111) compared to Ag(111).

## Experimental and theoretical details

### *Experimental Details*

**Materials and general methods:** Reagents were purchased at reagent grade from Acros and Sigma-Aldrich and used without further purification. Analytical TLC analysis was performed on aluminum plates coated with 0.20 mm silica gel containing a fluorescence indicator obtained from Macherey-Nagel; visualization with a UV lamp (254 or 366 nm). Column chromatography was performed on silica gel (230–400 mesh). The synthesis of 2,6,10-tribromo-4,4,8,8,12,12-hexamethyl-4*H*,8*H*,12*H*-benzo[1,9]quinolizino[3,4,5,6,7-*defg*]acridine (**2**) was performed according to the literature procedure.[20] Melting points were determined in open capillaries on a Büchi M-560 melting-point apparatus and are uncorrected; "decomp." refers to decomposition. $^{1}$H and $^{13}$C NMR spectra were recorded on Bruker Avance 300 and 400 spectrometers and referenced to the residual solvent signal as internal reference ($^{1}$H: $CD_2Cl_2$ 5.32 ppm; $^{13}$C: $CD_2Cl_2$ 53.8 ppm). Chemical shift values are reported in parts per million (ppm) relative to the signal of tetramethylsilane (TMS). Coupling constants (*J*) are given in Hz. The apparent resonance multiplicity is described as s (singlet), d (doublet), t

(triplet), q (quartet), and m (multiplet). Infrared spectra (IR) were recorded on a 660-IR (Varian, ATR mode) spectrometer, characteristic IR absorptions were reported in $cm^{-1}$ and denoted as strong (s), medium (m), and weak (w). UV/vis measurements were acquired on a Cary 5000 UV-Vis-NIR (Varian) spectrophotometer in a quartz cuvette (1 cm) at room temperature. The absorption maxima ($\lambda_{max}$) are reported in nanometers with the extinction coefficient ($\varepsilon$) in $M^{-1}\ cm^{-1}$ in parentheses. High-resolution mass spectra were obtained from a MicrOTOF II (Bruker, HR-ESI-MS) mass spectrometer at the Institute of Organic Chemistry, University Erlangen-Nürnberg. The signal of the molecular ion $[M]^+$ is reported in *m*/*z* units.

**4,4,8,8,12,12-Hexamethyl-4*H*,8*H*,12*H*-benzo[1,9]quinolizino[3,4,5,6,7-*defg*]acridine-2,6,10-tricarbonitrile (1):** A mixture of **2** (70 mg, 0.12 mmol) and CuCN (177 mg, 1.98 mmol) in dry *N*-methyl-2-pyrrolidone (5.0 mL) was heated at 180 °C for 72 hours. After cooling to r.t., the mixture was diluted with $H_2O$ (50 mL), adjusted to pH 2 with aq. HCl (1 M) and extracted with $CH_2Cl_2$ (3 × 20 mL). The combined organic layers were washed with $H_2O$ (3 × 20 mL), dried ($MgSO_4$), filtered, and the solvents were removed *in vacuo*. The crude product was purified by CC ($SiO_2$, $CH_2Cl_2$) to afford **1** (41 mg, 77%) as a white solid. $R_f$ = 0.46 ($SiO_2$, $CH_2Cl_2$); m.p. 232 °C (decomp.); $^1$H NMR (300 MHz, $CD_2Cl_2$): $\delta$ = 1.63 (s, 18 H), 7.72 ppm (s, 6 H); $^{13}$C NMR (75 MHz, $CD_2Cl_2$): $\delta$ = 33.13, 36.20, 108.66, 119.48, 128.52, 131.61, 134.56 ppm; IR (neat): $\tilde{\nu}$ = 2966 (w), 2923 (w), 2200 (m), 1597 (w), 1428 (s), 1288 (s), 1174 (m), 1092 (m), 1019 (m), 872 (m), 799 $cm^{-1}$ (s); UV/vis ($CH_2Cl_2$): $\lambda_{max}$ ($\varepsilon$) = 257 (72700), 313 (59600), 349 (sh, 87500), 356 nm (90900 $M^{-1}\ cm^{-1}$); HR-ESI-MS: *m*/*z* calcd for $C_{30}H_{24}N_4Na^+$ $[M + Na]^+$: 463.1899; found: 463.1904.

**Sample preparation and measurements:** All experiments were performed under ultra-high vacuum (UHV). The metal single crystals purchased from MaTecK were cleaned by repeated cycles of argon-ion bombardment (1-1.5 keV) and subsequent annealing to 400 °C for Ag(111) and Au(111) and 450 °C for Cu(111). The molecules were sublimed in-situ onto the single crystals held at room temperature. The evaporation rate, which was between 0.3 ML $min^{-1}$ and 0.7 ML $min^{-1}$, was monitored by means of a quartz crystal microbalance. The STM experiments were performed in a two chamber UHV system equipped with a sample preparation chamber, containing a MCP LEED (Omicron NanoTechnology) and a second chamber housing a commercially available STM (Omicron NanoTechnology). All STM images were acquired at 77 K, unless otherwise stated, with a mechanically cut Pt/Ir wire in constant current mode. The tunnelling bias is given with respect to a grounded tip. WSxM was used to analyse the STM images.[41] The XPS experiments were performed in a separate UHV system equipped with a preparation chamber and an analysis chamber containing an Al $K_\alpha$/ Mg $K_\alpha$ twin anode x-ray gun and a hemispherical energy analyser (Thermo Fisher). The analysis chamber also houses a LEED optics (SPECS) and a commercially available STM (Omicron NanoTechnolgy), which was used at room temperature to calibrate the coverage before the XPS experiments were performed. Al $K_\alpha$ x-rays with a photon energy of 1461.6 eV were used for the XPS measurements. The Cu $2p_{3/2}$ and the Au $4f_{7/2}$ peak at 932.6 eV and 84.0 eV, respectively, were used for binding energy calibration.[42]

## *Theoretical Details*

All calculations were carried out within the framework of density functional theory (DFT), as embedded into the Vienna ab initio Simulation Package (VASP).[43] The calculations were performed using the generalized gradient approximation (GGA) in the form of Perdew-Burke-Ernzerhof (PBE)[44] as well as by including the non-local interactions through the self-consistent van der Waals DFT (optB88-vdW[45] functional) as implemented in the VASP package.[45] The interaction between the valence electrons and ionic cores is described by the projector augmented wave (PAW) method.[46] A kinetic-energy cutoff of 400 eV was used for the wave functions. The adsorption on Ag, Au, and Cu(111) surfaces was simulated by placing the molecule on one side of a (6 x 6) slab containing three layers with 19 Å of vacuum separating the two surfaces. The k-point mesh of 3 x 3 x 1 is used for these calculations. During the structural optimization, the atoms of the molecule as well as those of the first layer substrate atoms were allowed to relax. The bottom two layers of the substrate were kept fixed. The relaxation was done with a 0.01 eV $Å^{-1}$ force criterion. The adsorption energies of three different adsorption configurations were evaluated and only the most stable configuration is reported in the text.

## Acknowledgements

F. Song, T. A. Pham, F. Studener and L. Venema are acknowledged for help during the experiments. This work was supported by the Foundation for Fundamental Research on Matter (FOM), part of the Netherlands Organisation for Scientific Research (NWO), by the European Research Council (ERC-2012-StG 307760-SURFPRO), by NWO (Chemical Sciences, VIDI-grant No. 700.10.424 and VENI-grant No. 722.012.010). M.K. and U.M. acknowledge financial support by the Deutsche Forschungsgemeinschaft (DFG) as part of SFB 953 “Synthetic Carbon Allotropes”, the Cluster of Excellence “Engineering of Advanced Materials (EAM) at the University of Erlangen-Nürnberg, and the “Solar Technologies Go Hybrid” initiative of the Free State of Bavaria, Germany. AK acknowledges support from the U.S. Department of Energy Basic Energy Science under Contract No DE-FG02-11ER16243. The computational study used resources of the National Energy Research Scientific Computing Center, which is supported by the Office of Science of the U.S. Department of Energy under Contract No. DE-FG02-11ER16243.

**Keywords:** self-assembly, molecule-substrate interaction, cyano-groups, triarylamines, scanning probe microscopy

[1] G. Horowitz, *Adv. Mater.* **1998**, *10*, 365-377; b) Y. S. Zhao, H. Fu, A. Peng, Y. Ma, D. Xiao, J. Yao, *Adv. Mater.* **2008**, *20*, 2859-2876; c) S. Fukuzumi, T. Kojima, *J. Mater. Chem,* **2008**, *18*, 1427-1439.

[2] M. W. Hosseini, *Acc. Chem. Res.* **2005,** *38*, 313-323.

[3] a) J. V. Barth, J. Weckesser, C. Cai, P. Günter, L. Bürgi, O. Jeandupeux, K. Kern, *Angew. Chem. Int. Ed.* **2000**, *39*, 1230-1234; b) J. A. Theobald, N. S. Oxtoby, M. A. Phillips, N. R. Champness, P. H. Beton, *Nature* **2003**, *424*, 1029-1031; c) R. Otero, M. Schöck, L. M. Molina, E. Lægsgaard, I. Stensgaard, B. Hammer, F. Besenbacher, *Angew. Chem. Int. Ed.* **2005**, *44*, 2270-2275; d) A. Llanes-Pallas, M. Matena, T. Jung, M. Prato, M. Stöhr, D. Bonifazi, *Angew. Chem. Int. Ed.* **2008**, *47*, 7726-7730.

[4] T. Yokoyama, S. Yokoyama, T. Kamikado, Y. Pkuno, S. Mashiko, *Nature* **2001**, *413*, 619-621.

[5] a) N. Wintjes, J. Hornung, J. Lobo-Checa, T. Voigt, T. Samuely, C. Thilgen, M. Stöhr, F. Diederich, T. A. Jung, *Chem.-Eur. J.* **2008**, *14*, 5794-5802; b) M. Stöhr, S. Boz, M. Schär, M.-T. Nguyen, C. A. Pignedoli, D. Passerone, W. B. Schweizer, C. Thilgen, T. A. Jung, F. Diederich, *Angew. Chem. Int. Ed.* **2011**, *50*, 9982-9986.

[6] S. Beniwal, S. Chen, D. A. Kunkel, J. Hooper, S. Simpson, E. Zurek, X. C. Zeng, A. Enders, *Chem. Commun.* **2014**, *50*, 8659-8662.

[7] a) N. Lin, A. Dmitriev, J. Weckesser, J. V. Barth, K. Kern, *Angew. Chem. Int. Ed.* **2002**, *41*, 4779-4783; b) J. V. Barth, *Surf. Sci.* **2009**,

*603*, 1533-1542; c) C. S. Kley, J. Čechal, T. Kumagai, F. Schramm, M. Ruben, S. Stepanow, K. Kern, *J. Am. Chem. Soc.* **2012**, *134*, 6072-6075.

[8] G. M. Whitesides, J. P. Mathias, C. T. Seto, *Science* **1991**, *254*, 1312-1319.

[9] a) M. Alemani, S. Selvanathan, F. Ample, M.V. Peters, K.-H. Rieder, F. Moresco, C. Joachim, S. Hecht, L. Grill, *J. Phys. Chem. C* **2008**, *112*, 10509-10514; b) R. Gutzler, H. Walch, G. Eder, S. Kloft, W. M. Heckl, M. Lackinger, *Chem. Commun.* **2009**, 4456-4458; c) M. Bieri, M.-T. Nguyen, O. Gröning, J. Cai, M. Treier, K. Aït-Mansour, P. Rufieux, C. A. Pignedoli, D. Passerone, M. Kastler, K. Müllen, R. Fasel, *J. Am. Chem. Soc.* **2010**, *132*, 16669-16676; d) R. Otero, J. M. Gallego, A. L. Vázquez de Parga, N. Martín, R. Miranda, *Adv. Mater.* **2011**, *23*, 5148-5176.

[10] A. C. Papageorgiou, S. Fischer, J. Reichert, K. Diller, F. Blobner, F. Klappenberger, F. Allegretti, A. P. Seitsonen, J. V. Barth, *ACS Nano* **2012**, *6*, 2477-2486.

[11] L Romaner, D. Nabok, P. Puschnig, E. Zojer, C. Ambrosch-Draxl, *New J. Phys.* **2009**, *11*, 053010 (1-21).

[12] a) F. Buchner, E. Zillner, M. Röckert, S. Gläßel, H.-P. Steinrück, H. Marbach, *Chem. Eur. J.* **2011**, *17*, 10226-10229; b) H. Marbach, H.-P. Steinrück, *Chem. Commun.* **2014**, *50*, 9034-9048.

[13] a) E. I. Altmann, R. J. *Colton, Surf. Sci.* **1993**, *295*, 13-33; b) T. Hashizume, K. Motai, X. D. Wang, H. Shinohara, Y. Saito, Y. Matuyama K. Ohno, Y. Kawazoe , Y. Nishina, H. W. Pickering, Y. Kuk, T. Sakurai, *Phys. Rev. Lett.* **1993**, *71*, 2959-2962; c) E. I . Altmann, R. J. Colton, *Phys. Rev. B* **1993**, *48*, 18244-18249; d) J. K. Gimzewski, S. Modesti, T. David, R. R. Schlittler, *J. Vac. Soc. Technol. B* **1994**, *12*, 1942-1946; e) T. David, J. K. Gimzewski, D. Purdie, B. Reihl, R. R. Schlittler, *Phys. Rev. B* **1994**, *50*, 5810-5813; f) T. Sakurai, X.-D. Wang, Q.K. Zue, Y. Hasegawa, T. Hashizume, H. Shinohara, *Prog. Surf. Sci.* **1996**, *51* ,263-408.

[14] L.-A. Fendt, M. Stöhr, N. Wintjes, M. Enache, T. A. Jung, F. Diederich, *Chem. Eur. J.* **2009**, *15*, 11139-11150.

[15] A. Shchyrba, M.-T. Nguyen, C. Wäckerlin, S. Martens, S. Nowakowska, T. Ivas, J. Roose, T. Nijs, S. Box, M. Schär, M. Stöhr, C. A. Pignedoli, C. Thilgen, F. Diederich, D. Passerone, T. A. Jung, *J. Am. Chem. Soc.* **2013**, *135*, 15270-15273.

[16] J. Reichert, M. Marschall, K. Seufert, D. Ecija, W. Auwärter, E. Arras, S. Klyatskaya, M. Ruben, J. V. Barth, *J. Phys. Chem. C* **2013**, *117*, 12858-12863.

[17] T. Sirtl, S. Schlögl, A. Rastoo-Lahrood, J. Jelic, S. Neogi, M. Schnittel, W. M. Heckl, K. Reuter, M. Lackinger, *J. Am. Chem. Soc.* **2013**, *135*, 691-695.

[18] S. Klyatskaya, F. Klappenberger, U. Schlickum, D. Kühne, M. Marschall, J. Reichert, R. Decker, W. Krenner, G. Zoppellaro, H. Brune, J. V. Barth, M. Ruben, *Adv. Funct. Mater.* **2011**, *21*, 1230-1240.

[19] a) J. E. Field, D. Venkataraman, *Chem. Mater.* **2002**, *14*, 962-964; b) N. S. Makarov, S. Mukhopadhyay, K. Yesudas, J.-L. Brédas, J. W. Perry, A. Pro, M. Kivala, K. Müllen, *J. Phys. Chem. A* **2012**, *116*, 3781-3793; c) F. Schlütter, F. Rossel, M. Kivala, V. Enkelmann, J.-P. Gisselbrecht, P. Ruffieux, R. Fasel, K. Müllen, *J. Am. Chem. Soc.* **2013**, *135*, 4550-4557; d) N. Hammer, T. A. Schaub, U. Meinhardt, M. Kivala, *Chem. Rec.* **2015**, DOI: 10.1002/tcr.201500202.

[20] Z. Fang, T.-L. Teo, L. Cai, Y.-H. Lai, A. Samoc, M. Samoc, *Org. Lett.* **2009**, *11*, 1-4.

[21] S. Gottardi, K. Müller, J. C. Moreno Lopéz, H. Yildirim, U. Meinhardt, M. Kivala, A. Kara, M. Stöhr, *Adv. Mater. Interfaces* **2014**, *1*,1300025 (1-10).

[22] M. Bieri, S. Blankenburg, M. Kivala, C. A. Pignedoli, P. Ruffieux, K. Müllen, R. Fasel, *Chem. Commun.* **2011**, *47*, 10239-10241.

[23] Y. Okuno, T. Yokoyama, S. Yokoyama, T. Kamikado, S. Mashiko, *J. Am. Chem. Soc.* **2002**, *124*, 7218-7225.

[24] a) S. M. Barlow, R. Raval, *Surf. Sci. Rep.* **2003**, *50*, 201-341; b) K.-H. Ernst, *Phys. Status Solidi B* **2012**, *249*, 2057-2088.

[25] a) A. Stabel, R. Heinz, F.C. De Schryver, J. P. Rabe, *J. Phys. Chem.* **1995**, *99*, 505-507; b) A. Murgarza, N. Lorente, P. Ordejón, C. Krull, S. Stepanow, M.-L. Bocquet, J. Fraxedas, G. Ceballos, P. Gambardella, *Phys. Rev. Lett.* **2010**, *105*, 115702 (1-4).

[26] Note that for **1** on Ag(111) the right handed chirality is shown (Figure 1) while for **1** on Au(111) the left handed chirality is shown (Figure 2a and b).

[27] a) M. A. Fortes, *Phys. Status Solidi B* **1972**, *54*, 311-319; b) D. E. Hooks, T. Fritz, M. D. Ward, *Adv. Mater.* **2001**, *13*, 227-241.

[28] J. Björk, M. Matena, M. S. Dyer, M. Enache, J. Lobo-Checa, L. H. Gade, T. A. Jung, M. Stöhr, M. Persson, *Phys. Chem. Chem. Phys.* **2010**, *12*, 8815-8821.

[29] M. Matena, J. Björk, M. Wahl, T.-L. Lee, J. Zegenhagen, L. H. Gade, T. A. Jung, M. Persson, M. Stöhr, *Phys. Rev. B* **2014**, *90*, 125408 (1-8).

[30] The full-width half maximum (FWHM) of the peaks has been kept free for the fits. They are all in the range of 1.5-2.1 eV except the one at lowest binding energy for 0.85 ML on Cu(111) which has a full width half maximum of 2.6 eV. For the data measured on Au(111) the background of the clean gold has been subtracted.

[31] T.-C. Tseng, C. Urban, Y. Wang, R. Otero, S. L. Tait, M. Alcamí, D. Écija, M. Trelka, J. M. Gallego, N. Lin, M. Konuma, U. Starke, A. Nefedov, A. Langner, C. Wöll, M. Á. Herranz, F. Martín, N. Martín, K. Kern, R. Miranda, *Nature Chem.* **2010**, *2*, 374-379.

[32] P. Fesser, C. Iacovita, C. Wäckerlin, S. Vijayaraghavan, N. Ballav, K. Howes, J.-P. Gisselbrecht, M. Crobu, C. Boudon, M. Stöhr, T. A. Jung, F. Diederich, *Chem. Eur. J.* **2011**, *17*, 5246 – 5250.

[33] T.-C. Tseng, C. Lin, X. Shi, S. L. Tait, X. Liu, U. Starke, N. Lin, R. Zhang, C. Minot, M. A. Van Hove, J. I. Cerdá, K. Kern, *Phys Rev. B* **2009**, *80*, 155458 (1-6).

[34] a) H. Yildirim, T. Greber, A. Kara, *J. Phys. Chem. C* **2013**, *117*, 20572-20583; b) H. Yildirim, A. Kara, *J. Phys. Chem. C* **2013**, *117*, 2893-2902; c) J. Matos, T. Rojas, H. Yildirim, A. Kara, *J. Chem. Phys.* **2014**, *140*, 144703; d) J. Matos, H. Yildirim, A Kara, *J. Phys. Chem. C* **2015**, *119*, 1886-1897.

[35] Van der Waals radii: $d_{vdW,Cu}$: 1.40 Å, $d_{vdW,Ag}$: 1.72 Å, $d_{vdW,Au}$: 1.66 Å, $d_{vdW,N}$: 1.55 Å. The values have been taken from http://periodictable.com/Properties/A/VanDerWaalsRadius.v.html

[36] Note that the values for Au(111) differ slightly to those given in Ref. 21, because a different starting configuration led to this slightly more stable configuration.

[37] a) J. V. Barth, J. Weckesser, C. Cai, P. Günter, L. Bürgi, O. Jeandupeux, K. Kern, *Angew. Chem. Int. Ed.* **2000**, *39*, 1230-1234; b) M. Alemani, S. Selvanathan, F. Ample, M. V. Peters, K.-H. Rieder, F. Moresco, C. Joachim. S. Hecht, L. Grill, *J. Phys. Chem. C* **2008**, *112*, 10509-10514.

[38] a) M. N. Faraggi, N. Jiang, N. Gonzalez-Lakunza, A. Langner, S. Stepanow, K. Kern, A. Arnau, *J. Phys. Chem. C* **2012**, *116*, 24558-24565; b) B. Cui, H.-J. Yan, D. Wang, L.-J. Wan, *J. Electroanal. Chem.* **2013**, *688*, 237-255.

[39] G. Antczak, W. Kamiński, K. Morgenstern, *J. Phys. Chem. C* **2015**, *119*, 1442-1450.

[40] a) D. Venkataraman, S. Lee, J. S. Moore, P. Zhang, K. A. Hirsch, G. B. Gardner, A. C. Covey, C. L. Prentice, *Chem. Mater.* **1996**, *8*, 2030-2040; b) W. Choe, Y.-H. Kiang, Z. Xu, S. Lee, *Chem. Mater.* **1999**, *11*, 1776-1783; c) A. Erxleben, *CrystEngComm*, **2002**, *4*, 472–477; d) J. Ni, K.-J. Wei, Y. Liu, X.-C. Huang, D. Li, *Cryst. Growth Des.* **2010**, *10*, 3964-3976; e) P. Niranjana, A. Pati, S. K. Porwal, V. Ramkumar, S. J. Gharpure, D. K. Chand, *CrystEngComm*, **2013**, *15*, 9623–9633; f) C. S. Hawes, S. R. Batten, D. R. Turner, *CrystEngComm,* **2014**, *16*, 3737-3748.

[41] I. Horcas, R. Fernández, J. M. Gómez-Rodríguez, J. Colchero, J. Gómez-Herrero, A. M. Baro, *Rev. Sci. Instr.* **2007**, *78*, 013705 (1-8).

[42] J. F. Moulder, W. F. Stickle, P. E. Sobol, K. D. Bomben, Handbook of X-ray Photoelectron Spectroscopy; Ed.: J. Chastain, Perkin-Elmer, Eden Prairie, Minnesota, USA **1992**.

[43] a) G. Kresse, J. Furthmüller, *Phys. Rev. B* **1996**, *54*, 11169; b) G. Kresse, J. Furthmüller, *Comput. Mater. Sci.* **1996**, *6*, 15-50.

[44] J. P. Perdew, K. Burke, M. Ernzerhof, *Phys. Rev. Lett.* **1996**, *77*, 3865-3868.

[45] J. Klimeš, D. R. Bowler, A. Michaelides, *J. Phys. Condens. Matter* **2010**, *22*, 022201 (1-5).

[46] a) P. Blöchl, *Phys. Rev. B* **1994**, *50*, 17953; b) G. Kresse, D. Joubert, *Phys. Rev. B* **1999**, *59*, 1758-1775.

**Entry for the Table of Contents** (Please choose one layout)

Layout 2:

FULL PAPER

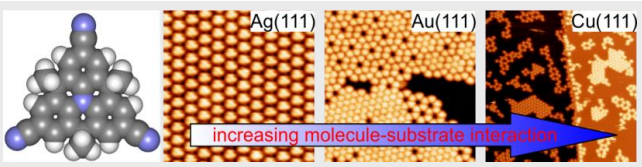


The self-assembly of cyano-functionalized triarylamine molecules was studied on (111) oriented coinage metal surfaces by means of scanning tunnelling microscopy, low-energy electron diffraction, X-ray photoelectron spectroscopy and density functional theory calculations. The subtle interplay between intermolecular and molecule-substrate interactions and the molecular mobility on the surfaces strongly influence the molecular self-assembly.

*K. Müller*, J.-C. Moreno-López, S. Gottardi, U. Meinhardt, H. Yildirim, A. Kara, M. Kivala*, M. Stöhr**

***Page No. – Page No.***
**Cyano-Functionalized Triarylamines on Coinage Metal Surfaces: Interplay of Intermolecular and Molecule-Substrate Interactions**